

HeTDSE: A GPU based program to solve the full-dimensional time-dependent Schrödinger equation for two-electron helium subjected to strong laser fields

Xi Zhao(赵曦), Gangtai Zhang(张刚台), Tingting Bai(白婷婷), Jun Wang(王俊), and Wei-Wei Yu(于伟威)
Citation: Chin. Phys. B, 2021, 30 (**7**): 073201. DOI: 10.1088/1674-1056/abe1a4
Journal homepage: http://cpb.iphy.ac.cn; http://iopscience.iop.org/cpb

What follows is a list of articles you may be interested in

Ultrafast photoionization of ions and molecules by orthogonally polarized intense laser pulses: Effects of the time delay

Si-Qi Zhang(张思琪), Zhi-Jie Yang(杨志杰), Zhi-Xian Lei(雷志仙), Wei Feng(冯伟), Sheng-Peng Zhou(周胜鹏), Kai-Jun Yuan(元凯军), Xue-Shen Liu(刘学深), and Jing Guo(郭静)
Chin. Phys. B, 2021, 30 (**1**): 013201. DOI: 10.1088/1674-1056/abb30c

Imprint of transient electron localization in H_2^+ using circularly-polarized laser pulse

Jianghua Luo(罗江华), Jun Li(李军), and Huafeng Zhang(张华峰)
Chin. Phys. B, 2020, 29 (**12**): 123201. DOI: 10.1088/1674-1056/abbbe1

Nonadiabatic molecular dynamics simulation of ${{\rm{C}}}_{2}{{\rm{H}}}_{2}^{2+}$ in a strong laser field

Ji-Gen Chen(陈基根), Gang-Tai Zhang(张刚台), Ting-Ting Bai(白婷婷), Jun Wang(王俊), Ping-Ping Chen(陈平平), Wei-Wei Yu(于伟威)§, and Xi Zhao(赵曦)¶
Chin. Phys. B, 2020, 29 (**11**): 113202. DOI: 10.1088/1674-1056/abb3de

Numerical simulations of strong-field processes in momentum space

Yan Xu(徐彦), Xue-Bin Bian(卞学滨)
Chin. Phys. B, 2020, 29 (**2**): 023202. DOI: 10.1088/1674-1056/ab6553

Bohmian trajectory perspective on strong field atomic processes

Xuan-Yang Lai(赖炫扬), Xiao-Jun Liu(柳晓军)
Chin. Phys. B, 2020, 29 (**1**): 013205. DOI: 10.1088/1674-1056/ab5c0f

---

HeTDSE: A GPU based program to solve the full-dimensional time-dependent Schrödinger equation for two-electron helium subjected to strong laser fields*

Xi Zhao(赵曦)[1,5,6], Gangtai Zhang(张刚台)[2,†], Tingting Bai(白婷婷)[3], Jun Wang(王俊)[4,‡], and Wei-Wei Yu(于伟威)[7,§]

[1] *School of Physics and Information Technology, Shaanxi Normal University, Xi'an* 710062, *China*
[2] *College of Physics and Optoelectronics Technology, Baoji University of Arts and Sciences, Baoji* 721016, *China*
[3] *College of Mathematics and Information Science, Baoji University of Arts and Sciences, Baoji* 721013, *China*
[4] *Institute of Atomic and Molecular Physics, Jilin University, Changchun* 130012, *China*
[5] *Department of Physics, Kansas State University, Manhattan, KS* 66506, *USA*
[6] *School of Physics and Electronics, Qiannan Normal College for Nationalities, Duyun* 558000, *China*
[7] *School of Physics and Electronic Technology, Liaoning Normal University, Dalian* 116029, *China*

(Received 10 August 2020; revised manuscript received 27 January 2021; accepted manuscript online 1 February 2021)

Electron–electron correlation plays an important role in the underlying dynamics in physics and chemistry. Helium is the simplest and most fundamental two-electron system. The dynamic process of helium in a strong laser field is still a challenging issue because of the large calculation cost. In this study, a graphic processing unit (GPU) openACC based *ab initio* numerical simulations package HeTDSE is developed to solve the full-dimensional time-dependent Schrödinger equation of helium subjected to a strong laser pulse. HeTDSE uses B-spline basis sets expansion method to construct the radial part of the wavefunction, and the spherical harmonic functions is used to express for the angular part. Adams algorithm is employed for the time propagation. Our example shows that HeTDSE running on an NVIDIA Kepler K20 GPU can outperform the one on an Intel E5-2640 single CPU core by a factor of 147. HeTDSE code package can be obtained from the author or from the author's personal website (doi: 10.13140/RG.2.2.15334.45128) directly under the GPL license, so HeTDSE can be downloaded, used and modified freely.

Keywords: strong field physics, TDSE, OPENACC, GPU, electron correlation, helium

PACS: 32.80.Rm, 42.50.Hz, 42.65.Ky **DOI:** 10.1088/1674-1056/abe1a4

1. Introduction

The rapid development in laser technologies opens a way for scientists to probe and even control the fundamental dynamics of electron correlations.[1–21] As the simplest multi-electron atom, helium is an idea starting point for exploring electron correlation dynamics in multi-electron systerms.[14,25–41] However, due to its six degrees of freedom, the response of helium to strong fields is considerably more complicated than that of single-electron atoms, which poses great theoretical and computational challenge. To overcome this difficulty, a set of conventional CPU parallel computing techniques have been developed to numerically solve the time-dependent Schrödinger equation (TDSE) of helium subjected to a laser pulse. Peng *et al.* investigated the electron correlation effects in two-photon-double-ionization (TPDI) of helium by the finite-element-discrete-variable-representation (FEDVR) method.[39] Parker *et al.* used the finite-difference method to calculate the above-threshold ionization (ATI) process.[40] Piraux *et al.* investigated the electron correlation effect using the Gauss–Sturman function.[30] All of these simulations are very likely a numerical virtual experiment on the servers (about 200 to 1000 CPU cores are used in Refs. [39,40]). Thus, more efficient algorithm is needed to further promote the numerical simulations of helium (and even more complex multi-electron systems beyond helium) in strong laser field investigations. One of the potential solution is the graphic processing unit (GPU) programming, which is the most powerful high performance computing tool so far and widely applied in both science and engineering numerical studies.[43–50]

GPU contains hundreds of computing cores and is originally designed for highly parallel process of graphic rendering.[43,44] Compared with CPU, the computing perfor-

*Project supported the National Natural Science Foundation of China (Grant Nos. 11904192, 11604119, 11627807, and 11604131), the Natural Science Basic Research Plan of Shaanxi Province of China (Grant No. 2016JM1012), the Natural Science Foundation of the Education Committee of Shaanxi Province of China (Grant No. 18JK0050), the Science Foundation of Baoji University of Arts and Sciences of China (Grant No. ZK16069), and the Natural Science Foundation of Liaoning Province of China (Grant No. LQ 2020022).

†Corresponding author. E-mail: gtzhang79@163.com
‡Corresponding author. E-mail: wangjun86@jlu.edu.cn
§Corresponding author. E-mail: weiweiyu2012@163.com

© 2021 Chinese Physical Society and IOP Publishing Ltd

mance of GPU can be increased by tens of times with proper optimizing.[43–50] To do this, a so-called "Compute Unified Device Architecture (CUDA)" GPU programming model is present.[44] However, porting of legacy CPU-based codes with CUDA often necessitates explicit compute and data management, thus requiring significant structural changes to existing applications.[45] Therefore, we make the choice to use OpenACC, which gives an alternative model as a GPU programming scheme.[51] OpenACC is a set of directive-based extensions to C, C++ and Fortran that allow programmers to annotate regions of code and data for offloading from a CPU host to an attached GPU, without requiring modification to the underlying CPU code itself. Programmers simply insert OpenACC directives before specific code sections to engage the GPU to accelerate the code. This approach enables the compiler to target and optimize parallelism automatically. More example programs and detailed description of openACC can be found in openACC official website.[51]

In this work, we present a GPU based openACC fortran program HeTDSE, which is an efficient tool to investigate the non-perturbative electronic dynamics of helium subjected to a strong laser pulse by solving full-dimensional two-electron TDSE. It goes beyond the single-electron-approximation (SEA) approach and includes the response to the field of all two electrons. To build helium wavefunction, B-spline basis sets, which were widely used in computational atomic and molecular physics,[21,52–62] are used to construct the radial part of the wavefunction, while spherical harmonic functions are used to express for the angular part. The reason why we use B-spline basis sets to expand helium radial wavefunction is that B-spline function has great advantages of describing both bound and continue states with small number basis sets.[52,53,55] Adams algorithm is employed for the time propagation.[63] Another advantage of using B-spline basis sets and Adams method is that it is easy to parallelize the code and will get an excellent paralleling scaling with openACC.

The rest of this paper is organized as follows: In Section 2, we present the theoretical background on HeTDSE. In Section 3 we exhibit an overview of the package structure, the input, output files and the code parallelizing. In Section 4 we show several test applications of HeTDSE. The parallel efficiency is given in Section 5. We present our conclusions in Section 6. Atomic units are used throughout, unless stated otherwise.

2. Mathematical setup and algorithm

2.1. B-spline function

B-splines are functions designed to generalize polynomials for the purpose of approximating arbitrary functions, we use B-spline basis sets to construct the helium wavefunction in HeTDSE. Thus, we begin this section with a brief description of B-spline function, very details of B-spline function can be found in Ref. [55].

A B-spline function is defined by the order k and a set of the breakpoints $\{t_j\}$,

$$B_{j,1}(r) = \begin{cases} 1, & t_j \le r \le t_{j+1}, \\ 0, & \text{otherwise}, \end{cases}$$
$$B_{j,k}(r) = \frac{r-t_j}{t_{j+k-1}-t_j} B_{j,k-1} + \frac{t_{j+k}-r}{t_{j+k}-t_{j+1}} B_{j+1,k-1}. \quad (1)$$

The radial coordinates of helium wavefunction is discrete in the interval $[r_{\min}, r_{\max}]$ by the breakpoints $\{t_j\}$. Three types of breakpoints sequence $\{t_j\}$ are used in HeTDSE.[55] The first one is a linear sequence

$$t_j = r_{\min} + (r_{\max} - r_{\min}) \frac{j-1}{n-1}. \quad (2)$$

The sequence is divided into equal lengths.

The second is an exponential sequence,

$$t_j = r_{\min} + (r_{\max} - r_{\min}) \frac{e^{\gamma\left(\frac{j-1}{n-1}\right)} - 1}{e^{\gamma} - 1}, \quad j = 1, \ldots, n. \quad (3)$$

This sequence tends to a linear sequence as $\gamma \to 0$ while all points exponentially accumulate close to $r_{\min}$ as $\gamma \to \infty$.

The third is a linear-parabolic sequence. A useful sequence adapted to a good description of both the bound and the continuum states associates to a linear spreading at large distances with a quadratic sequence close to the origin.[55]

$$t_j = \begin{cases} r_{\min} + \alpha(j_0 - 1)^2, & 1 \le j < j_0, \\ r_0 + \beta(j - j_0), & j_0 \le j \le n, \end{cases} \quad (4)$$

where $r_0 = \frac{r_{\max}(i_0-1) + r_{\min}(n-i_0)}{2n-i_0-1}$, $\alpha = \frac{r_0 - r_{\min}}{(i_0-1)^2} n$ and $\beta = \frac{r_{\max} - r_0}{n - i_0} n$. The parameter j_0 defines the value of j at which the connection is made. Other types sequences can be found in Ref. [55] and references therein.

The derivative of a B-spline of order k can be expressed as a linear combination of B-splines of the same order,

$$\frac{dB_{j,k}(r)}{dr} = \frac{k-1}{t_{j+k-1} - t_i} B_{j,k-1}(r) - \frac{k-1}{t_{j+k} - t_i} B_{j+1,k-1}(r). \quad (5)$$

The B-spline function order $k = 7$ is used throughout this work, so we do not write out k in B-spline functions for simplification.

2.2. Time independent Schrödinger equation

The helium eigenstate $\varphi_n(r_1, r_2)$ and its corresponding eigenvalue E_n is the solution to the time-independent Schrödinger Eq. (TISE) of helium:

$$H_0(r_1, r_2)\, \varphi_n(r_1, r_2) = E_n \varphi_n(r_1, r_2), \quad (6)$$

with $H_0(\boldsymbol{r}_1,\boldsymbol{r}_2)$ being the laser-free Hamiltonian

$$H_0(\boldsymbol{r}_1,\boldsymbol{r}_2) = -\frac{\nabla_1^2}{2} - \frac{\nabla_2^2}{2} - \frac{2}{r_1} - \frac{2}{r_2} - \frac{1}{|\boldsymbol{r}_1-\boldsymbol{r}_2|}, \tag{7}$$

where $-\nabla_i^2/2 - 2/r_i$ with $i = 1,2$ denoting the kinetic energy and potential energy of electron i, and $\frac{1}{|\boldsymbol{r}_1-\boldsymbol{r}_2|}$ is the electron-electron correlation term. The time-independent helium wavefunction is expanded as

$$\begin{aligned}\varphi_n(\boldsymbol{r}_1,\boldsymbol{r}_2) =& \sum_{i=1}^{N} c_i[B_{n_1}(r_1)B_{n_2}(r_2)Y_{l_1l_2}^{LM}(\hat{r}_1,\hat{r}_2) \\ &+(-1)^{l_1+l_2+L+S}B_{n_1}(r_2)B_{n_2}(r_1)Y_{l_1l_2}^{LM}(\hat{r}_2,\hat{r}_1)],\end{aligned} \tag{8}$$

where N is the number of the B-spline basis sets for each time-independent wavefunction $\varphi_n(\boldsymbol{r}_1,\boldsymbol{r}_2)$, $l_1(l_2)$ denotes the angular momenta for electron $1(2)$, L is the total orbital angular momentum, M is its z-component, S is the total spin, $\{c_i\}$ is the expansion coefficient, and each i corresponds to a set of $\{n_1,l_1,n_2,l_2\}$. Coupled spherical harmonic functions are used to express for the angular part of the time-independent wavefunction:

$$\begin{aligned}Y_{l_1l_2}^{LM} =& \sum_{m_1m_2}(-1)^{l_1-l_1+L}\sqrt{2L+1}\begin{pmatrix} l_1 & l_2 & L \\ m_1 & m_2 & -M\end{pmatrix} \\ &\times Y_{l_1m_1}(\hat{r}_1)Y_{l_2m_2}(\hat{r}_2),\end{aligned} \tag{9}$$

where $m_1(m_2)$ is the z-component of $l_1(l_2)$, and $Y_{lm}(\hat{r})$ is usual spherical harmonic functions.

The wavefunction $\varphi_n(\boldsymbol{r}_1,\boldsymbol{r}_2)$, eigenvalue E_n as well as the expansion coefficient $\{c_i\}$ in Eq. (8) can be obtained by directly diagonalizing Eq. (6). For this purpose, there are a set of matrix integrals that would be performed: the kinetic energy integral matrix element

$$K_{ij} = \int_{r_{\min}}^{r_{\max}} B_j(r)\frac{\mathrm{d}^2}{\mathrm{d}r^2}B_i(r)\,\mathrm{d}r, \tag{10}$$

the potential energy integral matrix element

$$P_{ij} = \int_{r_{\min}}^{r_{\max}} B_j(r)\frac{B_i(r)}{r}\,\mathrm{d}r, \tag{11}$$

the overlap integral

$$O_{ij} = \int_{r_{\min}}^{r_{\max}} B_j(r)B_i(r)\,\mathrm{d}r, \tag{12}$$

and the coupling term integral

$$C_{ij} = \int_{r_{\min}}^{r_{\max}} B_j(r_1)\frac{B_i(r_1)}{|\boldsymbol{r}_1-\boldsymbol{r}_2|}\,\mathrm{d}r_1, \tag{13}$$

K_{ij}, P_{ij} and O_{ij} are straightforward to discretize and to be calculated. However, the calculation of C_{ij} is different. To calculate C_{ij} we expand the electron-electron correlation term in a truncated multipole series:

$$\frac{1}{|\boldsymbol{r}_1-\boldsymbol{r}_2|} \approx \sum_l\sum_m \frac{4\pi}{2l+1}\frac{r_<^l}{r_>^{l+1}}Y_{lm}^*(\hat{r}_1)Y_{lm}(\hat{r}_2). \tag{14}$$

Thus, each of the terms is handled in a similar manner to the one-electron operators.[53] In HeTDSE, all the integrals are carried by the Gauss–Lagrange integration method, which has been widely used in other works.[41]

2.3. The time-dependent Schrödinger equation

We solve the helium TDSE within the dipole approximation and length gauge. The full-dimension TDSE of helium can be written as

$$\mathrm{i}\frac{\partial}{\partial t}\Psi(\boldsymbol{r}_1,\boldsymbol{r}_2,t) = H(\boldsymbol{r}_1,\boldsymbol{r}_2,t)\Psi(\boldsymbol{r}_1,\boldsymbol{r}_2,t), \tag{15}$$

where the total Hamiltonian of the atom-laser system is

$$H(\boldsymbol{r}_1,\boldsymbol{r}_2,t) = H_0(\boldsymbol{r}_1,\boldsymbol{r}_2) + H_I(t). \tag{16}$$

The interaction Hamiltonian of the helium and laser pulse is

$$H_I(t) = (\boldsymbol{r}_1+\boldsymbol{r}_2)\cdot\boldsymbol{e}(\boldsymbol{t}) = -(\boldsymbol{r}_1+\boldsymbol{r}_2)\cdot\partial\boldsymbol{A}(\boldsymbol{t})/\partial t, \tag{17}$$

where the vector potential of the laser pulse is

$$\boldsymbol{A}(\boldsymbol{t}) = \hat{\varepsilon}A_0\,f(t)\sin(\omega t+\phi)/\omega. \tag{18}$$

Here $\hat{\varepsilon}$ is the laser polarization direction, ω and ϕ are the frequency and the carrier envelope phase, respectively; and $f(t)$ is the temporal envelope.

The total time-dependent wavefunction $\Psi(\boldsymbol{r}_1,\boldsymbol{r}_2,t)$ can be expanded in terms of the field-free atomic eigenfunctions:

$$\Psi(\boldsymbol{r}_1,\boldsymbol{r}_2,t) = \sum_{s=1}^{N_{\text{total}}} a_s(t)\,\mathrm{e}^{-\mathrm{i}E_st}\varphi_s(\boldsymbol{r}_1,\boldsymbol{r}_2). \tag{19}$$

Here N_{total} is the total number of the wavefunction $\varphi_n(\boldsymbol{r}_1,\boldsymbol{r}_2)$. Substituting Eq. (19) into Eq. (15), the TDSE is converted into a set of coupled partial differential equations:

$$\begin{aligned}\mathrm{i}\frac{\mathrm{d}}{\mathrm{d}t}a_n(t) =& \sum_m a_m(t)\,\mathrm{e}^{-\mathrm{i}E_{mn}t} \\ &\times\langle\varphi_n(\boldsymbol{r}_1,\boldsymbol{r}_2)|\,(r_1Y_{10}(\hat{r}_1)+r_2Y_{10}(\hat{r}_2)) \\ &\times|\varphi_m(\boldsymbol{r}_1,\boldsymbol{r}_2)\rangle\frac{\partial\boldsymbol{A}(t)}{\partial t},\end{aligned} \tag{20}$$

which can be solved with the Adams method. Details of this algorithm can be found in Ref. [63]. The energy difference $E_{mn} = E_m - E_n$ and the transition dipole element between $\langle\varphi_n(\boldsymbol{r}_1,\boldsymbol{r}_2)|$ and $|\varphi_m(\boldsymbol{r}_1,\boldsymbol{r}_2)\rangle$,

$$d_{nm} = \langle\varphi_n(\boldsymbol{r}_1,\boldsymbol{r}_2)\,|\,(r_1Y_{10}(\hat{r}_1)+r_2Y_{10}(\hat{r}_2))|\,\varphi_m(\boldsymbol{r}_1,\boldsymbol{r}_2)\rangle \tag{21}$$

can be calculated from the solution to Eq. (6).

2.4. Absorbing boundary

An absorbing layer $A(r_1, r_2)$ is used to smoothly bring down the wavefunction and to prevent the unphysical reflection from the boundary. The absorbing function has the following form:

$$A(r_1, r_2) = \begin{cases} 1, & r_{\min} \le R \le r_{\text{mask}}, \\ \cos^{\frac{1}{8}}\left(\frac{\pi(R-r_{\text{mask}})}{2(r_{\max}-r_{\text{mask}})}\right), & r_{\text{mask}} \le R \le r_{\max} w, \end{cases} \quad (22)$$

where $R = \sqrt{r_1^2 + r_2^2}$. The default value of r_{mask} is set to $r_{\text{mask}} = r_{\max} - 10$. Alternatively, users can change this value by themselves. The helium time-dependent wave function $\Psi(\boldsymbol{r}_1, \boldsymbol{r}_2, t)$ multiplies the absorbing boundary $A(r_1, r_2)$ at each time step in the time propagation.

Thus, there are two interpretations of the ionization yield. First, we directly calculate the single (double) ionization yield by summing all the possibilities of the wavefunction with an eigenvalue larger than $-2.0(0.0)$:

$$Y(t) = \sum_{i}^{E_i \ge -2.0(0.0)} |c_i(t)|^2. \quad (23)$$

Alternatively, the ionization probability is calculated by

$$Y(t) = 1 - \langle \Psi(\boldsymbol{r}_1, \boldsymbol{r}_2, t) | \Psi(\boldsymbol{r}_1, \boldsymbol{r}_2, t) \rangle. \quad (24)$$

Although we have used an absorbing to avoid the non-physical reflecting, the simulation box still needs to be set big enough so that the physical system is not perturbed by the absorbing boundaries.

3. Description of the package

HeTDSE code package contains 9 fortran files and 4 input files. The fortran driver programs, functions, subroutines, input and output files are all introduced briefly in this section.

3.1. Fortran program files

These fortran codes should be run one by one: Firstly, running *eigen-equation.f* to solve Eq. (6) to get wavefunction $\varphi_n(\boldsymbol{r}_1, \boldsymbol{r}_2)$, eigenvalue E_n as well as the expansion coefficient $\{c_i\}$. Then, with the output files of *eigen-equation.f*, running *dipole.f90* to get the transition dipoles element $\langle \varphi_n(\boldsymbol{r}_1, \boldsymbol{r}_2) | (r_1 Y_{10}(\hat{r}_1) + r_2 Y_{10}(\hat{r}_2)) | \varphi_m(\boldsymbol{r}_1, \boldsymbol{r}_2) \rangle$. Next, running *matrix.f90* to prepare input files for *tdse.f90*. Finally, running *tdse.f90* to solve Eq. (20) to get the time-dependent wavefunction $\Psi(\boldsymbol{r}_1, \boldsymbol{r}_2, t)$.

There are other five fortran programs *order.f*, *rsg.f*, *wig.f*, *angl16.f90* and *SUBROUTINE.f90* in HeTDSE. These five programs are the "support codes", we DO NOT suggest the users to modulate them.

3.2. Lower-level functions and subroutines

The lower-level functions and subroutines in this program are:

PREQUAN: Get the index of the one electron functions $B_n(r) Y_{lm}$ from 1 to $n \times (l_{\max} + 1)$.

QUAN2012: Select the basis sets that satisfies physics considerations: the one electron angular momenta l_1, l_2 should satisfy $|l_1 - l_2| \le L \le |l_1 + l_2|$ and the wavefunction $\Psi(r_1, r_2) \ne 0$.

gauleg: Calculate the Gauss–Lagrange integration.

DBSP2: Calculate the second derivative of the B-spline function $\mathrm{d}^2 B_n(r) / \mathrm{d}r^2$.

DBSP1: Calculate the first derivative of the B-spline function $\mathrm{d}B_n(r) / \mathrm{d}r$.

RKTSQ: Set the breakpoints distribution.

Bspline2006: Calculate the B-spline function $B_n(r)$.

SingleInteg2012: Calculate the integration P_{ij}, K_{ij} or O_{ij}.

DmultiInteg2012: Calculate the electron-electron integration C_{ij}.

HAMILTON2012: Construct the Hamiltonian.

RSG: Diagonalize the matrix, get the energy level and wavefunctions.

ANG: Calculate the angle part of transition dipole element.

ode: Solve Eq. (20) by Adams algorithm.

f: Define the vector potential Eq. (18).

F3J0: Calculate 3-J symbol $\begin{pmatrix} j_1 & j_2 & j_3 \\ m_1 & m_2 & m_3 \end{pmatrix}$.

F6J: Calculate 6-J symbol $\begin{Bmatrix} j_1 & j_2 & j_3 \\ j_4 & j_5 & j_6 \end{Bmatrix}$.

abr: Set the absorbing boundary.

3.3. Input files

There are totally four input files in HeTDSE, *eigen-equation.input*, *dipole.input*, *matrix.input* and *tdse.input*, which contain input parameters used by *eigne-equation.f*, *dipole.f90*, *matrix.f90* and *tdse.f90*, respectively. In this subsection, we present how to set these parameters in these input files one by one.

Eigen-equation.input

Line 1: Set total angular momentum L in Eq. (8).

Line 2: Set total spin in Eq. (8).

Line 3: Set max angular momentum for each electron $l_{\max}$.

Line 4: Set the order of the B-spline function k.

Line 5: Set number of B-SPLINE function breakpoints, that is to say, n in Eqs. (2), (3), and (4).

Line 6: Set total number of the basis sets for the He wavefunction N in Eq. (8).

Line 7: i_0 in Eq. (4).

Line 8: Set the simulation box size in radial direction, $r_{\max}$.

Dipole.input

Line 1: Set total angular momentum L of $\langle\varphi_n(\boldsymbol{r}_1,\boldsymbol{r}_2)|$ and $|\varphi_m(\boldsymbol{r}_1,\boldsymbol{r}_2)\rangle$ in Eq. (8), respectively.

Line 2: Set total spin M of $\langle\varphi_n(\boldsymbol{r}_1,\boldsymbol{r}_2)|$ and $|\varphi_m(\boldsymbol{r}_1,\boldsymbol{r}_2)\rangle$ in Eq. (8), respectively.

Lines 3–8 in *dipole.input* are the same as lines 3–8 in *eigen-equation.input*.

Matrix.input

First values in lines 1, 2, 3 and 4: The numbers of the basis sets used in TDSE of states are $L=0$, $L=1$, $L=2$, $L=3$ and $L=4$, respectively.

Second values in lines 1, 2, 3 and 4: The total numbers of the basis sets of states are $L=0$, $L=1$, $L=2$, $L=3$ and $L=4$, respectively.

The default max total angular momentum is $L=4$, larger total angular momentums can be added in this input file, if needed.

Tdse.input

User should not change lines 1 and 2 in *tdse.input*, so we skip them and begin with line 3.

Line 3: The maximum number of time steps allowed. Default value is 600000.

Line 4: Frequency of the electric field in atomic unit.

Line 5: Number of the laser cycles.

Line 6: Intensity of the electronic laser field in atomic unit.

Line 7: Relative and absolute errors. Default values are 10^{-7} and 10^{-7}, respectively.

3.4. Output files

Output files of eigen-equation.f:

There are two output files after running *eigen-equation.f*: the coefficient c_i $(i=1,\ldots,N)$ of the wavefunction $\varphi_n(r_1,r_2)$, and the eigenvalue E_n.

1. *S.dat*: This file stores the coefficient c_i in Eq. (6). The file name would change to *P.dat*, *D.dat*, *F.dat* and *G.dat* if $L=1,2,3,4$, respectively.

2. *OMEGA-S.dat*: This file stores the eigenvalue E_n of states with $\varphi_n(r_1,r_2)$. The file name would change to *OMEGA-P.dat*, *OMEGA-D.dat*, *OMEGA-F.dat*, *OMEGA-G.dat* if $L=1,2,3,4$, respectively.

Output files of dipole.f90

There is one output file after running *dipole.f90*: the transition dipole moment elements between a pair of states with neighbouring total angular momentums L and $L+1$.

Output files of matrix.f90:

There are three output files after running *matrix.f90*:

1. *eigenval.out*: This file stores all the eigenvalues in the order $L=0,1,2,3,4$.

2. *HI.dat*: This files stores all the dipole matrix elements.

3. *OMEGA.dat*: This files stores all the energy differences.

Output files of tdse.f90

There are four output files after running *tdse.f90*:

1. *laser.dat*: This file stores laser field $E(t)$.

2. *single-ion.dat*: This file stores the single ionization yield $I_s(t)$.

3. *double-ion.dat*: This file stores the double ionization yield $I_d(t)$.

4. *c.dat*: This file stores the solution $a_n(t)$ $(n=1,\ldots,N_{\text{total}})$ to the coupled partial differential equation (20) at each time step. In principle, if we obtain $a_n(t)$, all the physical information can be retrieved.

3.5. OpenACC parallelizing implementation

In this subsection, we detailedly explain the OpenACC implementation in HeTDSE. In HeTDSE package, more than 99% computation time would be paid to calculate transition dipole moment d_{mn} and time propagation. Thus, we focus on accelerating the two calculations with openACC. In *dipole.f90* programs, four do-loops are needed to get all the transition dipole moment elements d_{mn} (see Eq. (21) for mathematical expression), and each loop would run 2000–10000 times. The code and corresponding openACC accelerated implementation is shown below:

```
!$ACC KERNELS
    do m=1, NUMS
     do n=1, NUMP
       sum=0.d0
       do i=1, NUMS
            do j=1, NUMP
sum=sum+TERM(i,j)*c1(i,m)*c1p(j,n)
          end do
       end do
dipole(m,n)=sqrt(4.d0*pi/3.d0)*sum
      end do
    end do
!$ACC END KERNELS
```

Although the computing scale is large, the code structure itself is really simple (nothing but a sum calculation) and openACC can achieve a high performance parallelizing scaling. All four do-loops are parallelized directly by inserting the OpenACC directive "!$ACC KERNELS", then the data transfer between the host and the GPU memory is automatically executed. The calculation in the area (line 2 to line 12) of directive is executed and accelerated on GPU. Optimization for time propagation is similar, here is the Adams time propagation code at each time step and corresponding openACC accelerated implementation:

```
!$ACC PARALLEL LOOP PRIVATE(m,n)
do n=1,nhi
```

```
    ap(n)=0
    do m=1,nhi
ap(n)=ap(n)+sin(omega(n,m)&
&*t)*hi(n,m)*a(m)
    end do
    do m=nhi+1,neq
ap(n)=ap(n)+cos(omega(n,m-nhi)&
&*t)*hi(n,m-nhi)*a(m)
    end do
end do
!$ACC END PARALLEL LOOP
```

As we know, the data transfer between the host and GPU memory affects the computational time. To further minimize the cost of data transfer, we use the OpenACC "DATA COPY" before time propagating starts, and "END DATA" is used to release the GPU memory at the end of time propagating:

```
!$ACC DATA COPY( hi,omega )
call ode(f,neq,a,t,&
    &tout,relerr,abserr,iflag,work,iwork)
!$ACC END DATA
```

The datacopy (namelist) is the directive that copies the data from host to GPU memory, then data on GPU memory is used without the data transfer back and forth between the host and GPU every time step. Clearly, by inserting datacopy, the calculational time is much saved.

The advantages of using B-spline basis set and Adams method in HeTDSE are emphasized again at the end of this section: First, it is convenient to implement openACC. Second, the parallelizing scaling has a high performance, which will be shown in Section 5.

4. Sample results

In order to verify the accuracy of our program, we compare our results with previous literatures. In the calculations, the radius of the cavity is $r_{\max} = 70$, $r_{\min} = 0$ for both electrons and it is described by 30 B-spline functions of order 7. We use $l_{i=1,2} = 0, 1, 2, 3, 4$ and $L = 0, 1, 2, 3, 4$ in below simulation examples. Linear-parabolic breakpoints sequence is chosen. Total number of basis sets $N_{\text{total}} = 11000$ are used during the time-dependent simulations. r_{mask} in absorbing boundary is set to $r_{\text{mask}} = 60$. It should mention here that choosing such parameters is because we can get a convergence in the ionization calculation in Subsection 4.3. For the other calculations, such as ground/bound states calculations and excited states dynamics simulations, we do not need to use a radius as large as 70.

4.1. Ground and bound states calculation of helium

In Table 1, we show the eigenvalues of few low bound states for different total angular momenta. Table 1 shows that, for all the calculated levels, at least the accuracy up to two digits after the decimal point has been obtained. Specifically, we compare our ground state eigenvalue with a more accurate method from Ref. [22]. In Ref. [22], Kinoshita used 39 parameters and finally obtained a eignvalue of -2.9037225, which is only 0.0036935 of difference from our result. This small difference indicates that the accuracy from our method is acceptable.

Table 1. The energy level of some bound states.

Helium states	Our results	Ref. [59]	Ref. [42]
1^1S	–2.900029	–2.903531	–2.903724
2^1S	–2.145044	–2.145961	–2.145974
3^1S	–2.060512	–2.061268	–2.061371
4^1S	–2.032866	–2.033585	–2.033586
2^1P	–2.123121	–2.123832	–2.123843
3^1P	–2.054443	–2.055143	–2.055146
3^1D	–2.054927	–2.055621	–2.055620
4^1D	–2.030586	–2.031280	–2.031280
4^1F	–2.030562	–2.031255	–2.031255
5^1F	–2.019272	–2.020003	–2.020003

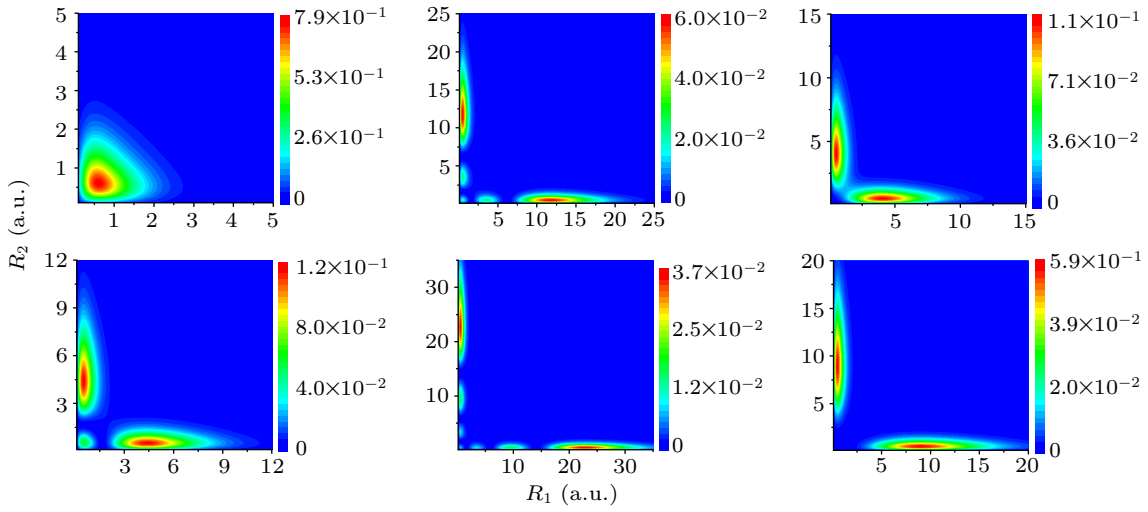


Fig. 1. The density distributions of some bound states in coordinate space.

The density distributions $d_e(R_1,R_2)$ of different atomic levels are calculated via $d_e(R_1,R_2) = \int R_1^2 R_2^2 \varphi(R_1,R_2)\,\varphi^*(R_1,R_2)\,\mathrm{d}\Omega_1\,\mathrm{d}\Omega_2$, which are shown in Fig. 1, where the results agree well with those in Refs. [14,21,59]. In Fig. 1, the nucleus are always set to be at the origin.

The effects of two-electron correlation coming from electron-electron repulsion have been a important subject from the early days of quantum mechanics, the relative position r_{12} of two electrons are even more important than their absolute positions for some purposes. Thus it is necessary to reduce the two-electron density further. The first specific calculation in respect of this was performed by Coulson and Neilson who deduced the expression for the distribution function of the inter-electronic distance r_{12},[23]

$$f_c(r_{12}) = 8\pi^2 r_{12}\left\{\int_{r_{12}}^{\infty} r_1\,\mathrm{d}r_1 \int_{r_1-r_{12}}^{r_1+r_{12}} r_2\varphi_i^2(R_1,R_2)\,\mathrm{d}r_2 + \int_0^{r_{12}} r_1\,\mathrm{d}r_1 \int_{r_{12}-r_1}^{r_{12}+r_1} r_2\varphi_i^2(R_1,R_2)\,\mathrm{d}r_2\right\}, \quad (25)$$

$f_c(r_{12})$ is called the position-space intracule and normalized to unity by $\int_0^{\infty} f_c(r_{12})\,\mathrm{d}r_{12} = 1$. We show our result of $f_c(r_{12})$ in Fig. 2, the position peak appears at about 1.2, which is in good agreement with the corresponding values computed by Curl and Coulson using 10-term Hylleraas basis sets.[24]

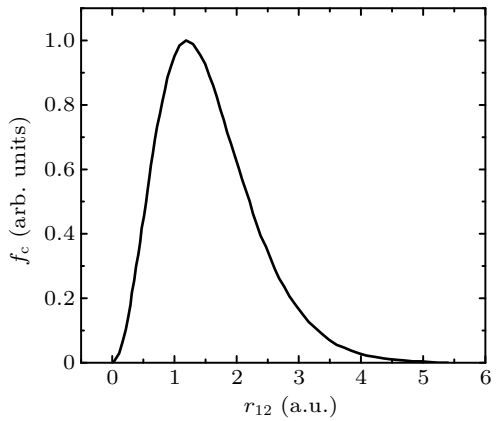


Fig. 2. The intracule density $f_c(r_{12})$ as a function of r_{12}.

4.2. Excited states dynamics

Now we turn to the second example: excited states dynamics. We focus on the carrier-envelope phase (CEP) effect on band-band state transition induced by a laser pulse. The CEP is a crucial parameter in describing the characteristics of a laser pulse, we can control the dynamic process of matter-laser interaction by measuring or adjusting the CEP.[64–69] Especially, the CEP effect on the bound-bound transition of an atom has been investigated theoretically and experimentally.[64–69] Here we try to reproduce the result from Ref. [67]. In Ref. [67], the authors used Hylleraas coordinates to reconstruct the wavefunction of helium, and they introduced a parameter M to quantify the CEP effect:

$$M = \frac{P(\phi_{\max}) - P(\phi_{\min})}{[P(\phi_{\max}) + P(\phi_{\min})]^2}, \quad (26)$$

where $P(\phi_{\max})$ and $P(\phi_{\min})$ are, respectively, the maximum and minimum populations for a given excited state. A large value of M corresponds to a strong CEP effect. In this simulation, the laser parameters are the same as those in Ref. [67]. We use HeTDSE to obtain the value M for ^1D state after the laser ends, as shown in Fig 3. Our result matches well with that in Fig. 1(b) from Ref. [67].

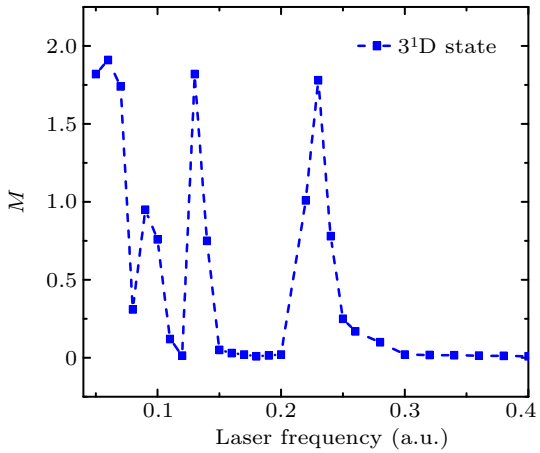


Fig. 3. The CEP parameter M vs the laser frequency for 3^1D state of helium.

4.3. Excitation and ionization yields

Next, we calculate the excitation and ionization yields of helium in a strong laser pulse. Our basis sets covers the energy range located beyond the double-ionization threshold. The initial state is the ground state of helium $|1S^2\rangle$. The laser pulse has a duration of 3.8 fs and the peak intensity of 2.97×10^{14} W/cm^2, which is the same as those in Refs. [54,59]. The present results in Fig. 4 are accordant with the data from Hasbani[54] and Scrinzi,[59] which certifies the accuracy of our code.

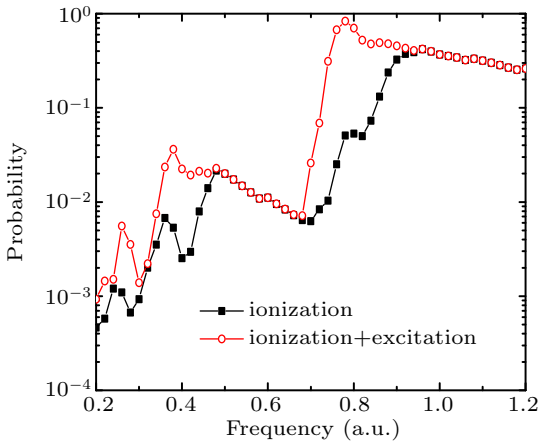


Fig. 4. Excitation and ionization probabilities, for the helium atom, with a pulse duration of 3.8 fs (fixed) and a peak intensity of 2.96×10^{14} W/cm^2.

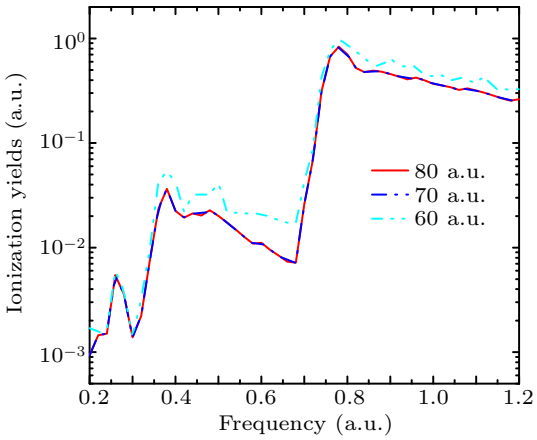


Fig. 5. Ionization yields for different simulation box $R = 80$ (red line), 70 (blue dotted line), and 60 (cyan dotted line), for the helium atom, the laser parameters are the same as those in Fig. 4.

The convergence of the radius is checked in Fig. 5. In Fig. 5, we choose three different simulation boxes $r_{\max} = 80$, $r_{\max} = 70$ and $r_{\max} = 60$, the absorbing boundary is set to 70, 60 and 50, respectively. In Fig. 5, we can see that ionization yields from $r_{\max} = 80$ and $r_{\max} = 70$ are almost same, in the meantime, the ionization yields from $r_{\max} = 60$ are much larger than those in the $r_{\max} = 80$ and $r_{\max} = 70$ cases. This result indicate that under such laser parameters, we can obtain a convergence with the radius equal to 70.

4.4. Electrons wavepacket dynamics

We then calculate the electrons wavepacket dynamics both in coordinate space after the laser pulse. The frequency and FWHM of the laser pulse are $\omega = 1.0$ and 2 optical cycles, respectively, with the intensity of 1.0×10^{13} W/cm^2, the electric field is shown in Fig. 6(b). The continue state is collected as $\psi_{\text{ion}} = \sum_i c_i \varphi_i$, with $E_i > -2.0$ a.u.

Using the time-dependent wave function, the density distribution of the electrons in coordinate space can be obtained by

$$\rho(r_1, r_2, t) = \int \Psi(\boldsymbol{r}_1, \boldsymbol{r}_2, t)\Psi^*(\boldsymbol{r}_1, \boldsymbol{r}_2, t) r_1^2 r_2^2 \, \mathrm{d}\Omega_1 \, \mathrm{d}\Omega_2. \quad (27)$$

Here $\Omega_{1(2)}$ is the angular part of the electron 1(2). The density distribution of continuous states in coordinate space is shown in Fig. 6(a) at the time T_{end} (which is labeled in Fig. 6(b)). We can see that there are evident single ionization characteristics from this figure.

Once the wavefunction at time t is obtained, we can also calculate the momentum distribution of the wavefunction with momentum k_1 and k_2 by Fourier transform

$$\Psi(k_1, k_2, t) = \int \mathrm{d}r_1^3 \, \mathrm{d}r_2^3 \, \mathrm{e}^{-\mathrm{i}k_1 r_1} \, \mathrm{e}^{-\mathrm{i}k_2 r_2} \Psi(r_1, r_2, t). \quad (28)$$

By expanding the plane wave $\mathrm{e}^{-\mathrm{i}k\cdot r}$ as

$$\mathrm{e}^{-\mathrm{i}k\cdot r} = 4\pi \sum_{lm} (-i)^l j_l(kr) Y_{lm}(k) Y_{lm}^*(r), \quad (29)$$

where $j_l(x)$ is sphere Bessel function,

$$j_l(x) = \sqrt{\frac{\pi}{2x}} J_{l+\frac{1}{2}}(x), \quad (30)$$

the density distribution in momentum space can be obtained by

$$P(k_1, k_2, t) = \int \Psi(k_1, k_2, t)\Psi^*(k_1, k_2, t) k_1^2 k_2^2 \, \mathrm{d}\Omega_1 \, \mathrm{d}\Omega_2. \quad (31)$$

, In order to check the accuracy of our code, we employ a two-color laser field with an intensity of $I = 1.0 \times 10^{12}$W/cm^2, the central energies are 36 eV and 80 eV, respectively, we calculate the momentum distribution after the laser ends in Fig. 7, the result coincides with the result from Ref. [21].

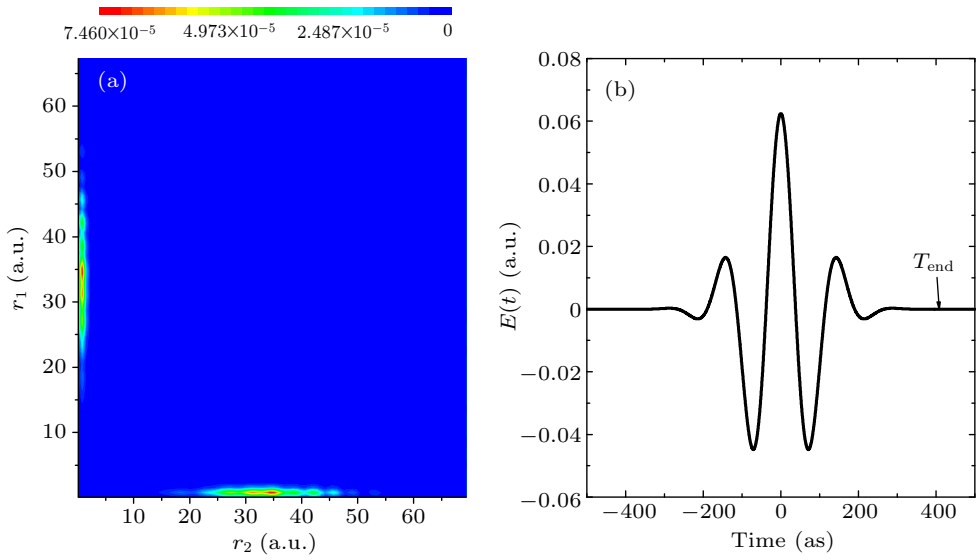


Fig. 6. The distributions of the continuum state in the coordinate space $\omega = 1.0$, FWHM = 2 OC, intensity $I = 1.0 \times 10^{13}$ W/cm^2 when the laser is ended.

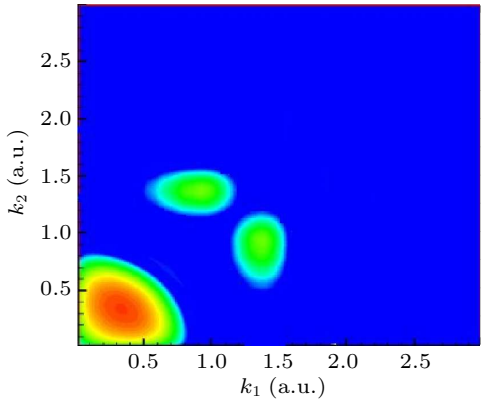


Fig. 7. The two-electron momentum distribution. We use a two-color laser field, in which the central energies are 36 eV and 80 eV, both the intensities are $I = 1.0 \times 10^{12}$ W/cm^2.

5. Parallel scaling

To test the parallel efficiency of HeTDSE, we compare the serial CPU program (runs at Intel xeon E5-2640 CPU with 2.5GHz clock speed and 15MB L3 cache) and parallel GPU implementations (runs at NVIDIA K20 GPU with 2493 cores). The speedup factor for four simulation cases is shown in Table 2. The larger the basis number, the larger computation cost needs. All the simulations are carried out with PGI fortran compiler, the laser is 3.8 fs (which contains about 4000 time steps) and the simulation box is $R_{\max} = 70$. A speed up of 147 is achieved if 4300 basis sets are used. It indicates that as the simulation system size increases, this improvement becomes more and more pronounced.

Table 2. The efficiency of our GPU program.

Basis number	GPU time (second)	CPU time (second)	Speed-up ratio
3000	41.22	3644.07	88.41
3600	48.61	4963.76	102.11
4200	60.06	7278.36	121.18
4800	86.26	12625.83	146.37

6. Conclusion

In this work, we have presented a program which solves the full-dimension-TDSE of helium using OpenACC+GPU simulation acceleration environment. We introduce how to convert the full-dimension-TDSE into coupled partial differential equations. These partial differential equations are solved by the Adams method. Our program has two advantages: Firstly, the codes are easily parallelled by adding few detectives and have a speed up of 147 on GPU, HeTDSE does not have to use a super computer or a computer cluster, even a desktop computer with an openACC-enable GPU can run HeTDSE efficiently. Secondly, we can transplant our program to other accelerators without rewriting the codes. By comparing with literature of the excited state dynamics and ionization yield of helium, the accuracy of our program has been verified. Our codes can be used to investigate the non-perturbative electronic dynamics of helium subjected to a strong laser pulse. In addition, for the programming for accelerators such as CUDA is difficult, we hope HeTDSE to be an example to help more researchers to handle the GPU calculation more easily using OpenACC.

References

[1] Xi Zhao's personal Researchgate website https://www.researchgate.net/publication/348786906_HeTDSE, with DOI: 10.13140/RG.2.2.15334.45128
[2] Shintake T *et al.* 2008 *Nat. Photon.* **2** 555
[3] Ackermann W *et al.* 2007 *Nat. Photon.* **1** 336
[4] Hentschel M, Kienberger R, Spielmann C, Reider G A, Milosevic N, Brabec T, Corkum P, Heinzmann U, Drescher M and Krausz F 2001 *Nature* **414** 509
[5] Paul P M, Toma E S, Breger P, Mullot G, Augé F, Balcou P, Muller H G and Agostini P 2001 *Science* **292** 1689
[6] Xia C L, Ge X L, Zhao X, Guo J and Liu X S 2012 *Phys. Rev. A* **85** 025802
[7] Guo J, Ge X L, Zhong H Y, Zhao X, Zhang M, Jiang Y F and Liu X S 2014 *Phys. Rev. A* **90** 053410
[8] Zhang J, Pan X F, Zhao X, Guo J, Zhu K G and Liu X S 2019 *J. Opt.* **21** 125503
[9] Zhao Y, Ma S, Jiang S, Yang Y, Zhao X and Chen J 2019 *Opt. Express* **27** 34392
[10] Zhao Y T, Xu X Q, Jiang S C, Zhao X, Chen J G and Yang Y J 2020 *Phys. Rev. A* **101** 033413
[11] Zhao Y T, Jiang S C, Zhao X, Chen J G and Yang Y J 2020 *Opt. Lett.* **45** 2874
[12] Qiao Y, Wu D, Chen J G, Wang J, Guo F M and Yang Y J 2020 *Phys. Rev. A* **100** 063428
[13] Jin C, Tang X, Li B, Wang K and Lin C D 2020 *Phys. Rev. Appl.* **14** 014057
[14] Zhang Z, Peng L Y, Xu M H, Starace A F, Morishite T and Gong Q H 2011 *Phys. Rev. A* **84** 043409
[15] Martin J M, Bade S, Dubosclard W, Khan M A, Kim S, Garraway B M and Alzar C L G 2019 *Phys. Rev. Appl.* **12** 014033
[16] Lopez C, Trimeche A, Comparat D and Picard Y J 2019 *Phys. Rev. Appl.* **11** 064049
[17] Guan J, Behrendt V, Shen P, Hofsass S, Muthu-Arachchige T, Grzesiak J, Stienkemeier F and Dulitz K 2019 *Phys. Rev. Appl.* **11** 054073
[18] Griesser H P, Perrella C, Light P S and Luiten A N 2019 *Phys. Rev. Appl.* **11** 054026
[19] Luo Y and Zhang P 2019 *Phys. Rev. Appl.* **12** 044056
[20] Chen P, Wang X, Luan Y, Fei Z, Lacroix B, Lei S and Das S R 2020 *J. Appl. Phys.* **128** 024305
[21] Zhang Z 2012 *PhD Dissertation* (Beijing: Peking University) (in Chinese)
[22] Kinoshita T 1956 *Phys. Rev.* **105** 1490
[23] Coulson C A and Neilson A H 1961 *Proc. Phys. Soc.* **78** 831
[24] Curl R F and Coulson C A 1965 *Proc. Phys. Soc.* **85** 647
[25] Colgan J and Pindzola M S 2002 *Phys. Rev. Lett.* **88** 173002
[26] Feng L and van der Hart H W 2003 *J. Phys. B* **36** L1
[27] Laulan S and Bachau H 2003 *Phys. Rev. A* **68** 013409
[28] Piraux B, Bauer J, Laulan S and Bachau H 2003 *Eur. Phys. J. D* **26** 7
[29] Hu S X, Colgan J and Collins L A 2005 *J. Phys. B* **38** L35
[30] Foumouo E, Kamta G L, Edah G and Piraux B 2006 *Phys. Rev. A* **74** 063409
[31] Guan X, Bartschat K and Schneider B I 2008 *Phys. Rev. A* **77** 043421
[32] Shi T Y and Lin C D 2002 *Phys. Rev. Lett.* **89** 163202
[33] Hasegawa H, Takahashi E J, Nabekawa Y, Ishikawa K L and Midorikawa K 2005 *Phys. Rev. A* **71** 023407
[34] Nabekawa Y, Hasegawa H, Takahashi E J andMidorikawa K 2005 *Phys. Rev. Lett.* **94** 043001
[35] Antoine P, Foumouo E, Piraux B, Shimizu T, Hasegawa H, Nabekawa Y and Midorikawa K 2008 *Phys. Rev. A* **78** 023415
[36] Sorokin A A, Wellhöfer M, Bobashev S V, Tiedtke K and Richter M 2007 *Phys. Rev. A* **75** 051402(R)

[37] Rudenko A, Foucar L, Kurka M, Ergler T, Kühnel K U, Jiang Y H, Voitkiv A, Najjari B, Kheifets A, Lüdemann S, Havermeier T, Smolarski M, Schssler S, Cole K, Schöffler M, Dörner R, Düsterer S, Li W, Keitel B, Treusch R, Gensch M, Schröter C D, Moshammer R and Ullrich J 2008 *Phys. Rev. Lett.* **101** 073003

[38] Kurka M *et al.* 2010 *New J. Phys.* **12** 073035

[39] Zhang Z, Peng L Y, Gong Q H and Morishite T 2010 *Opt. Express* **18** 8976

[40] Parker J S, Moore L R, Meharg K J, Dundas D and Taylor K T 2001 *J. Phys. B* **34** L69

[41] Zhang B, Yuan J and Zhao Z 2015 *Comput. Phys. Commun.* **194** 84

[42] Drake G W F 2006 *Springer Handbook of Atomic, Molecular and Optical Physics* (New York: Springer) pp. 205–206

[43] Thibault J C and Senocak I 2009 *CUDA Implementation of a Navier-Stokes Solver on Multi-GPU Desktop Platforms for Incompressible Flows* in *Proceedings of the 47th AIAA Aerospace Sciences Meeting* Orlando, Florida, USA,

[44] NVIDIA CUDA ZONE. https://developer.nvidia.com/cuda-zone. version 4.0, 2011

[45] Komura Y 2015 *Comput. Phys. Commun.* **197** 298

[46] Stone J E, Phillips J C, Freddolino P L, Hardy D J, Trabuco L G and Schulten K 2007 *J. Comput. Chem.***28** 2618

[47] Cheng W L, Sheharyar A, Sadr R and Bouhali O 2015 *Comput. Phys. Commun.* **182** 39

[48] Broin C and Nikolopoulos L A A 2014 *Comput. Phys. Commun.* **184** 1791

[49] Nguyen T D 2017 *Comput. Phys. Commun.* **212** 113

[50] Exl L 2017 *Comput. Phys. Commun.* **221** 352

[51] OpenACC official website. http://www.openacc-standard.org/

[52] Venuti M and Decleva P 1997 *J. Phys. B* **30** 4839

[53] Nepstad R, Birkeland T and Førre M 2010 *Phys. Rev. A* **81** 063402

[54] Hasbani R, Cormier E and Bachau H 2000 *J. Phys. B* **33** 2101

[55] Bachau H, Cormier E, Decleva P, Hansen J E and Martín F 2001 *Rep. Prog. Phys.* **64** 1815

[56] Zhao X, Wei H, Wu Y and Lin C D 2017 *Phys. Rev. A* **95** 043407

[57] Zhao X, Wei H, Wei C and Lin C D 2017 *J. Opt.* **19** 114009

[58] Shi T Y, Bao C G and Li B W 2001 *Commun. Theor. Phys.* **35** 195

[59] Scrinzi A and Piraux B 1998 *Phys. Rev. A* **58** 1310

[60] Yu W, Zhao X, Wei H, Wang S J and Lin C D 2019 *Phys. Rev. A* **99** 033403

[61] Zhao X, Wang S J, Yu W W, Wei H, Wei C, Wang B C, Chen J G and Lin C D 2020 *Phys. Rev. Appl.* **13** 034043

[62] Zhao X, Wei H, Yu W and Lin C D 2018 *Phys. Rev. A* **98** 053404

[63] Shampine L F and Gordon M K 1975 *Computer Solution of Ordinary Differential Equations: The Initial Value Problem* (San Francisco, CA: Freeman)

[64] Li H, Sautenkov V A, Rostovtsev Y V, Kash M M, Anisimov P M, Welch G R and Scully M O 2010 *Phys. Rev. Lett.* **104** 103001

[65] Zhao X, Chen J, Fu P, Liu X, Yan Z and Wang B 2013 *Phys. Rev. A* **87** 043411

[66] Zhao X, Yang Y, Liu X and Wang B 2014 *Chin. Phys. Lett.* **31** 043202

[67] Peng D, Wu B, Fu P, Wang B, Gong J and Yan Z C 2010 *Phys. Rev. A* **82** 053407

[68] Nakajima T and Watanabe S 2006 *Phys. Rev. Lett.* **96** 213001

[69] Zhai Z, Peng D, Zhao X, Guo F, Yang Y, Fu P, Chen J, Yan Z C and Wang B 2012 *Phys. Rev. A* **86** 043432